Rainbows from inhomogeneous transparent spheres: a ray-theoretic approach

John A. Adam and Philip Laven

A ray-theoretic account of the passage of light through a radially inhomogeneous transparent sphere has been used to establish the existence of multiple primary rainbows for some refractive index profiles. The existence of such additional bows is a consequence of a sufficiently attractive potential in the interior of the drop, i.e., the refractive index gradient should be sufficiently negative there. The profiles for which this gradient is monotonically increasing do not result in this phenomenon, but nonmonotone profiles can do so, depending on the form of n. Sufficiently oscillatory profiles can lead to apparently singular behavior in the deviation angle (within the geometrical optics approximation) as well as multiple rainbows. These results also apply to systems with circular cylindrical cross sections, and may be of value in the field of rainbow refractometry.

OCIS codes: 080.2710, 080.0080.

1. Introduction

This paper uses geometrical optics to analyze the scattering of light by inhomogeneous spheres in which the refractive index is a function of the radius only. The results may be of value in the field of rainbow refractometry and thermometry, which are optical techniques used to measure the refractive index (and hence the temperature) of transparent particles (including fuel droplets), and the cross-sectional shape of dielectric cylinders.[1–18] Such techniques can be used to determine very small spatial and time-varying changes in refractive index, and are valuable for analysis of the combustion of liquid hydrocarbons, the injection of sprays in high-pressure environments, as well as the spraying/drying techniques employed in the food, agricultural and pharmaceutical industries.[9] Gradients of refractive index can be caused when droplets undergo simultaneous heating and evaporation in a combustion chamber, and will be primarily radial if internal convection can be neglected compared with thermal conduction.[10] Similar refractometry studies have been carried out to determine the refractive indices and radii of unclad optical fibers.[19–21] While much of the work referenced above is based on geometrical optics, some utilize the more sophisticated Airy and/or Lorenz–Mie theories, explicitly or implicitly,[11,13–16] and most recently, generalizations of the Airy theory in combination with geometrical optics have been carried out.[22,23] The present study provides a basis for investigation of more complex radial gradients in refractive index than has hitherto been the case.

2. Rays in Radially Inhomogeneous Media

Using elementary differential geometry, it may be shown that if $\boldsymbol{\eta}$ is the radius vector of a point on a ray, and $\mathbf{s}$ is the tangent vector at that point, and $n(\eta)$ is the refractive index, then in terms of $\boldsymbol{\eta}$ and $\eta = |\boldsymbol{\eta}|$,

$$\boldsymbol{\eta} \times n(\eta)\mathbf{s} = \text{constant}. \tag{1}$$

This result, known as Bouguer's formula,[24] implies that all the ray paths are plane curves, in a plane through the origin, and that along each ray

$$n(\eta)\eta \sin \phi = \text{constant} = K, \tag{2}$$

where ϕ is the angle between the vector $\boldsymbol{\eta}$ and the tangent to the ray at that point. In a spherically symmetric medium, elementary geometry (in terms of the polar coordinates of a plane) indicates that

J. A. Adam is with the Department of Mathematics and Statistics at Old Dominion University, Norfolk, Virginia 23529. P. Laven (philip@philiplaven.com) can be contacted at Chemin de l'Avanchet 20, CH-1216 Cointrin, Geneva, Switzerland.

Received 10 July 2006; accepted 30 August 2006; posted 16 October 2006 (Doc. ID 72913); published 7 February 2007.

0003-6935/07/060922-08$15.00/0

$$\sin\phi = \frac{\eta(\theta)}{\sqrt{\eta^2(\theta) + (\mathrm{d}\eta/\mathrm{d}\theta)^2}}. \tag{3}$$

Equations (2) and (3) imply that

$$\frac{\mathrm{d}\eta}{\mathrm{d}\theta} = \pm\frac{\eta}{K}\sqrt{\eta^2 n^2(\eta) - K^2},$$

whence the governing equation for ray paths in spherically symmetric media is

$$\theta - \theta_0 = \pm K\int_R^{\xi} \frac{\mathrm{d}\eta}{\eta\sqrt{\eta^2 n^2(\eta) - K^2}}. \tag{4}$$

In this integral the upper limit of the radial variable η is the dummy variable ξ, where $0 \le \xi \le R$, R being the radius of the sphere. The initial angle θ_0 corresponds to the value of θ when $\xi = R$, namely at the point of entry of the ray into the sphere. To derive an expression for the total deviation $D(i)$ undergone by a ray after two refractions and one reflection, initially incident at angle i, that is a generalization of the primary rainbow ray path, the procedure is as follows. First consider $\eta'(\eta) < 0$ as in Fig. 1. By symmetry, $arcPQ = arcQS = arcST = arcTV$. As the ray moves along the path PQ from P to Q, θ is increasing while ξ is decreasing, so $\mathrm{d}\theta/\mathrm{d}\xi < 0$. Equivalently, if s is the arc length along the ray, $\mathrm{d}\theta/\mathrm{d}s > 0$ and $\mathrm{d}\xi/\mathrm{d}s < 0$ on this portion of the path. The $\theta = 0$ axis is oriented parallel to the incoming ray, thus $\theta_0 = i$, the angle of incidence. The total deviation along the path $PQSTV$ in this case is

$$D(i) = 2i + \pi - 4r(i) + \Theta, \tag{5}$$

where Θ is the deviation due to the nonzero curvature of the ray path. Thus Θ represents the excess deviation over the constant refractive index case, and by symmetry it is four times the excess deviation from P to Q. The exact shape of the path obviously depends on the choice for $n(\eta)$. It will be assumed that $n(\eta)$ is continuous in the interval (O, R). To elucidate the functional form of Θ, consider the point Q on the path, corresponding to the stationary angle $\bar{\theta}$ in the diagram, i.e., where

$$\left.\frac{\mathrm{d}\xi}{\mathrm{d}\theta}\right|_{\bar{\theta}} = 0. \tag{6}$$

Recall from Eq. (4) that

$$\frac{\mathrm{d}\theta}{\mathrm{d}\xi} = -\frac{K}{\xi\sqrt{\xi^2 n^2(\xi) - K^2}}.$$

The choice of $-K$, where $K > 0$ has been made because $\theta'(\xi) < 0$ on the portion PQ of the arc. Thus

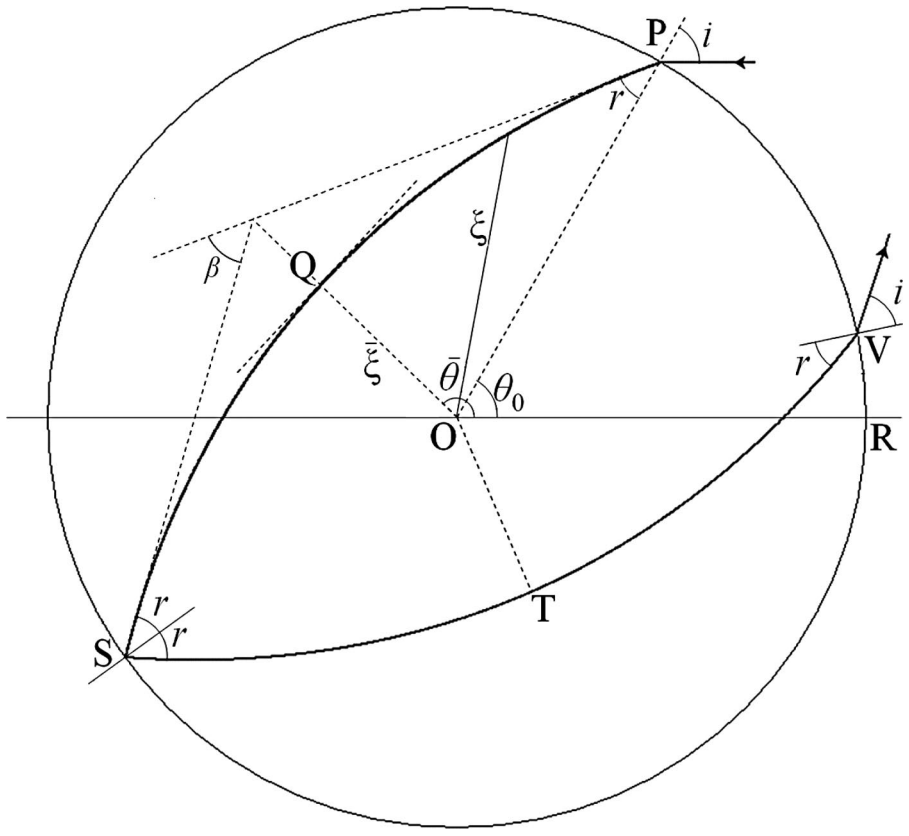

Fig. 1. Ray path for a single internal reflection; any point on the path is identified by its polar coordinates (ξ, θ).

condition (6) occurs when (i) $\xi = 0$, and (ii) more interestingly, when $\xi^2 n^2(\xi) = K^2$. This provides a natural definition of the turning point[25] $\bar{\xi}$, where $\bar{\xi} \equiv \xi(\bar{\theta})$; on arc PQ (or any equivalent arc) this mapping is invertible for a given sign of K, so we also have a more useful form $\bar{\theta} \equiv \theta(\bar{\xi})$. As can be seen from Fig. 1, this is the point at which a ray propagating into the droplet is refracted away from its closest point of entry to the center (in the case of constant n, the interior ray path is straight of course, but $\bar{\xi}$ still defines the point of closest approach to the origin.

It is convenient to employ a dimensionless version of some of the above equations in what follows, scaling radial distances within the sphere by the radius R. Let $\lambda = \eta/R$, $\bar{\lambda} = \bar{\xi}/R$, where $0 \le \bar{\lambda} \le \lambda \le 1$, and $\bar{K} = K/R$. At the point of entry P, the angle $\phi = r(i)$, the angle of refraction [see Eq. (2)]. The value of $\bar{K}$ determines the subsequent path of any incident ray. Since $n(\lambda)$ is discontinuous at $\lambda = 1$, it follows that

$$\bar{K}(i) = \lim_{\lambda \to 1^-} [\lambda n(\lambda)] \sin r(i) = \lim_{\lambda \to 1^-} \lambda \sin i = \sin i,$$

but when $\lambda = \bar{\lambda}$,

$$\bar{K} = \bar{\lambda} n(\bar{\lambda}) \sin\left[\phi(\bar{\lambda})\right] = \bar{\lambda} n(\bar{\lambda}) \sin[\pi/2] = \bar{\lambda} n(\bar{\lambda}),$$

so that in principle $\bar{\lambda}$ may be determined for a given refractive index profile from the result

$$\bar{K} = \bar{\lambda} n(\bar{\lambda}) = \sin i. \tag{7}$$

Notice also that in general the solution $\bar{\lambda}$ will not be unique, but in practice it should be straightforward to identify the physically significant one. From Eq. (4) for $\theta = \bar{\theta}$, in dimensionless terms

$$\bar{\theta} - i = -\bar{K} \int_1^{\bar{\lambda}} \frac{d\eta}{\eta \sqrt{\eta^2 n^2(\eta) - K^2}} = \bar{K} \int_{\bar{\lambda}}^1 \frac{d\lambda}{\lambda \sqrt{\lambda^2 \bar{n}^2(\lambda) - \bar{K}^2}} \equiv \bar{K} I(\bar{\lambda}, i), \tag{8}$$

where $\bar{n}(\lambda) = n(\eta)$. For any convex quadrilateral

$$\beta = -\pi + 2(r + \bar{\theta} - i), \tag{9}$$

(and so $\beta = 0$ when n = constant.) For the total path $PQSTV$, $\Theta = 2\beta$, from which it follows that for $n'(r) > 0$ the total deviation for a primary bow is, from Eq. (5)

$$D(i) = 2i - \pi + 4\bar{K} \int_{\bar{\lambda}}^1 \frac{d\lambda}{\lambda \sqrt{\lambda^2 \bar{n}^2(\lambda) - \bar{K}^2}}. \tag{10}$$

This result reduces to the known result for n = constant. Clearly, the integral in Eq. (10) is improper at the lower limit. This corresponds of course to the definition of $\bar{\lambda}$, the value of λ at which $\lambda'(\theta) = 0$; in practice, the integral exists for reasonable choices of $\bar{n}(\lambda)$. In the case for which $\bar{n}'(\lambda) < 0$, the curvature is away from the center, i.e., in the clockwise sense this time, so Eq. (5) still applies, but now β is defined as

$$\beta = \pi - 2(r + \bar{\theta} - i). \tag{9'}$$

3. Specific Refractive Index Profile

A specific monotonically decreasing profile for $\bar{n}(\lambda)$ will be chosen because it offers reasonable analytic tractability for the perturbation analysis in Section 4 and because it readily illustrates the double rainbow phenomenon. The choice of $\bar{n}(\lambda)$ was made because the gradient $\bar{n}'(\lambda)$ is not constant, thereby allowing for the possibility of subtle features that may not be present in a linear profile. While it may be argued that a linear profile is simpler to investigate, this is not in fact the case: The latter contains a quartic term in the radicand of the integral and results in elliptic integrals that, analytically at least, provide little insight into the physics of the problem; furthermore for this profile $\bar{\lambda}$ is not unique. The equation for $\bar{\lambda}$ in this case is admittedly only a quadratic, and it is physically obvious which root to take, but this lends a minor but additional complication to a less general and yet more complex case. Furthermore since any smooth profile can be can be reasonably approximated by a linear Taylor polynomial for a sufficiently small inhomogeneity, the choice of $\bar{n}(\lambda)$ below contains the linear profile as a special case. This idea is used in the perturbation analysis below: although $\bar{\lambda}$ is known exactly for this refractive index profile it is nonlinear in "sin i", and a linearization of $\bar{\lambda}$ about its value for n_0 for a homogeneous sphere is very useful in evaluating the integrals below. The choice for $\bar{n}(\lambda)$ is subject to the boundary conditions $\bar{n}(0) \equiv n_0$ and $\bar{n}(1) \equiv n_1$, where $n_0 > n_1$. This determines the parameters $a[=(n_0 - n_1)/n_0 n_1]$ and $b(=n_0^{-1})$ in the chosen profile

$$\bar{n}(\lambda) = (a\lambda + b)^{-1} \equiv \frac{n_0 n_1}{(n_0 - n_1)\lambda + n_1}. \tag{11}$$

The expression for the minimum impact parameter $\bar{\lambda}(i)$ is found by solving Eq. (7) to give

$$\bar{\lambda} = \frac{n_1 \sin i}{n_0 n_1 - (n_0 - n_1)\sin i}. \tag{12}$$

Because the numerator is increasing and the denominator is decreasing with i, it follows from Eq. (12) that $\bar{\lambda}$ is an increasing function of i on $(0, \pi/2)$. Now the integral in Eq. (10) reduces to

$$I(\bar{\lambda}, i) = \int_{\bar{\lambda}}^1 \frac{(a\lambda + b)d\lambda}{\lambda \sqrt{\lambda^2 - \bar{K}^2 (a\lambda + b)^2}} \equiv a I_A + b I_B, \tag{13}$$

where $I_A = \int_{\bar{\lambda}}^{1} \frac{d\lambda}{\sqrt{C\lambda^2 + B\lambda + A}}$, (14)

$$I_B = \int_{\bar{\lambda}}^{1} \frac{d\lambda}{\lambda\sqrt{C\lambda^2 + B\lambda + A}}, \quad (15)$$

$$C \equiv 1 - a^2\bar{K}^2 = \left(1 - \left[\frac{n_0 - n_1}{n_0 n_1}\right]^2 \sin^2 i\right) > 0,$$

$$B \equiv -2ab\bar{K}^2 = -2\left[\frac{n_0 - n_1}{n_0 n_1}\right]\sin^2 i,$$

$$A \equiv -b^2\bar{K}^2.$$

The positivity of C follows from the fact that $n_0 - n_1 < n_0 n_1$ always for $n_1 \geq 1$. The above integrals are standard forms, so Eq. (13) can be recast into $I(1, i) - I(\bar{\lambda}, i)$, where[26]

$$I(\lambda, i) = \frac{a \ln\left[2\sqrt{C(C\lambda^2 + B\lambda + A)} + 2C\lambda + B\right]}{\sqrt{C}} + \frac{b}{\sqrt{-A}} \arcsin \frac{2A + B\lambda}{\lambda\sqrt{B^2 - 4AC}}. \quad (16)$$

4. Perturbation Analysis

To illustrate the effects of slight nonhomogeneity in $n(\eta)$ the profile parameter a will be considered small and equal to ε, the expansion parameter in what follows. [This forces $n_1 = 5(5\varepsilon + 3)^{-1}$, but this presents no difficulty because $n_1 \geq 1$ provided $\varepsilon \leq 0.4$.] The integral (14) will be expanded in powers of ε and inserted into Eq. (10) for $D(i)$, retaining only terms up to $O(\varepsilon)$ in both individual expansions and the final result. Interestingly, terms of $O(\varepsilon^{1/2})$, $O(\varepsilon)$ and $O(\varepsilon^{3/2})$ arise, but the terms $O(\varepsilon^{1/2})$ vanish identically. Up to $O(\varepsilon)$, Eq. (14) is

$$I(\bar{\lambda}, i) = \int_{\bar{\lambda}}^{1} \left(a + \frac{b}{\lambda}\right)\left[\frac{1}{\sqrt{\lambda^2 - \bar{K}^2 b^2}} + \frac{2\varepsilon\lambda b\bar{K}^2}{\left(\lambda^2 - \bar{K}^2 b^2\right)^{3/2}}\right] d\lambda \equiv I_1 + I_2 + I_3 + I_4, \quad (17)$$

where the integrals I_k, $k = 1, 2, 3, 4$ for now will remain indefinite. They are[26]

$$I_1 = a\int \frac{d\lambda}{\sqrt{\lambda^2 - \bar{K}^2 b^2}} = a \ln\left(\lambda + \sqrt{\lambda^2 - \bar{K}^2 b^2}\right);$$

$$I_2 = b\int \frac{d\lambda}{\lambda\sqrt{\lambda^2 - \bar{K}^2 b^2}} = -\frac{1}{\bar{K}} \arcsin\left(\frac{\bar{K}b}{\lambda}\right);$$

$$I_3 = 2\varepsilon ab\bar{K}^2 \int \frac{\lambda d\lambda}{\left(\lambda^2 - \bar{K}^2 b^2\right)^{3/2}} = -\frac{2\varepsilon ab\bar{K}^2}{\sqrt{\lambda^2 - \bar{K}^2 b^2}};$$

$$I_4 = 2\varepsilon b^2\bar{K}^2 \int \frac{d\lambda}{\left(\lambda^2 - \bar{K}^2 b^2\right)^{3/2}} = -\frac{2\varepsilon\lambda}{\sqrt{\lambda^2 - \bar{K}^2 b^2}}.$$

Also Eq. (7) implies that

$$\bar{\lambda} = \left(\varepsilon\bar{\lambda} + b\right)\sin i, \qquad \text{i.e., } \bar{\lambda} = b \sin i(1 + \varepsilon \sin i) + O(\varepsilon^2). \quad (18)$$

The expression $(\lambda^2 - \bar{K}^2 b^2)^{1/2}$ appears in various ways in the above integrals. It is readily verified that $(\lambda^2 - \bar{K}^2 b^2)^{1/2} = \sqrt{2b\varepsilon^{1/2}} \sin^{3/2} i + O(\varepsilon^{3/2})$. After some algebra the definite integrals are as follows:

$$[I_1]_{\bar{\lambda}}^{1} = \varepsilon \ln\left(\frac{1 + \left(\lambda^2 - \bar{K}^2 b^2\right)^{1/2}}{b \sin i}\right) + O(\varepsilon^{3/2});$$

$$[I_2]_{\bar{\lambda}}^{1} = -\frac{1}{\bar{K}}\left[\arcsin(\bar{K}b) - \frac{\pi}{2} + (2\varepsilon \sin i)^{1/2}\right] + O(\varepsilon^{3/2});$$

$$[I_3]_{\bar{\lambda}}^{1} = O(\varepsilon^{3/2});$$

$$[I_4]_{\bar{\lambda}}^{1} = \left(\frac{2\varepsilon}{\sin i}\right)^{1/2} - \frac{2\varepsilon}{\left(1 - \bar{K}^2 b^2\right)^{1/2}} + O(\varepsilon^{3/2}).$$

These results are then substituted into Eq. (10), resulting in (to $O(\varepsilon)$)

$$D(i) = 2i - \pi + 4\bar{K}\left\{\varepsilon \ln\left(\frac{1 + \left(1 - \bar{K}^2 b^2\right)^{1/2}}{b \sin i}\right) - \frac{1}{\bar{K}}\left[\arcsin(\bar{K}b) - \frac{\pi}{2} + (2\varepsilon \sin i)^{1/2}\right] + \left(\frac{2\varepsilon}{\sin i}\right)^{1/2} - \frac{2\varepsilon}{\left(1 - \bar{K}^2 b^2\right)^{1/2}}\right\} + O(\varepsilon^{3/2})$$

$$\approx 2i + \pi - 4 \arcsin(\bar{K}b) + 4\varepsilon\bar{K} \times \left\{\ln\left(\frac{1 + \left(1 - \bar{K}^2 b^2\right)^{1/2}}{b \sin i}\right) - \frac{2}{\left(1 - \bar{K}^2 b^2\right)^{1/2}}\right\}$$

$$= 2i + \pi - 4 \arcsin(b \sin i) + 4\varepsilon \sin i \times \left\{\ln\left(\frac{1 + \left(1 - b^2 \sin^2 i\right)^{1/2}}{b \sin i}\right) - \frac{2}{\left(1 - b^2 \sin^2 i\right)^{1/2}}\right\}. \quad (18a)$$

$$\equiv D_h(i) + \varepsilon F(i),$$

where $F(i) = 4 \sin i\left\{\ln\left(\frac{1 + \left(1 - b^2 \sin^2 i\right)^{1/2}}{b \sin i}\right) - \frac{2}{\left(1 - b^2 \sin^2 i\right)^{1/2}}\right\}$,

and $D_h(i)$ is the deviation for the homogeneous sphere (this follows because $b = n_0^{-1}$), and $\varepsilon F(i)$ is the additional deviation, to $O(\varepsilon)$, owing to the nonhomogeneous refractive index. To determine where an extremum of $D(i)$ occurs (if it does) relative to the homogeneous case (occurring at $i = i_c$, say), let us use

first-degree Taylor polynomials in the following manner: clearly, since from Eq. (18a), it follows that $D'(i) = D_h'(i) + \varepsilon F'(i)$. Near $i = i_c$, $i = i_c + \delta$, say (with $|\delta|$ small compared to i_c), $F(i) \approx F(i_c) + \delta F'(i_c)$. Then $D'(i) \approx 0 + \delta D_h''(i_c) + \varepsilon F'(i_c)$ to first order in small quantities δ, ε. Since a necessary condition for the existence of extrema in $D(i)$ is $D'(i) = 0$, it follows that

$$\delta D_h''(i_c) + \varepsilon[F'(i_c) + \delta F''(i_c)] \approx 0, \qquad \text{or}$$

$$\delta \approx -\frac{\varepsilon F'(i_c)}{D_h''(i_c) + \varepsilon F''(i_c)} = -\frac{\varepsilon F'(i_c)}{D_h''(i_c)} + O(\varepsilon^2). \quad (19)$$

Elementary ray theory shows that $D_h''(i_c) > 0$, and $F'(i_c) < 0$ for $n_0 = 5/3$ (as is readily verified from Fig. 2), it follows that $\delta > 0$ in the vicinity of i_c, i.e., the extremum occurs at slightly higher values of i than compared with the homogeneous case. Indeed, from the general shape of $F(i)$ in Fig. 2 it may be seen that $F(i) > 0$ for $i \in (0, \mu)$, where $\mu \approx 0.429$ for $n_0 = 5/3$ and $F(i) < 0$ for $i \in (\mu, \pi/2]$. This is consistent with the fact that compared with the homogeneous sphere, according to Fig. 3, there is now a maximum of $D(i)$ in $(0, \mu)$, and the minimum of $D(i)$ in $(\mu, \pi/2]$ is lower, i.e., $D(i_{\min}) < D_h(i_c)$. The reason for this is that initially, $F(i)$ increases faster than $D_h(i)$ decreases, so $D(i)$ also increases, decreasing shortly thereafter (according to Fig. 3, at $i \approx 16.3°$). In Fig. 2 the solid curve $[F(i)]$ is drawn for $n_0 = 5/3$ while the dashed curve $[F1(i)]$ is for $n_0 = 2.5$. In Fig. 3, $\varepsilon = 0.25$ and $n_0 = 5/3$, but even for this relatively large nonuniformity the agreement between the exact TotD(i) and the linear approximation given by Eq. (18a) is reasonable for angles of incidence less than approximately 30°. The disparity between these two graphs shrinks (as one would expect) as ε tends to zero.

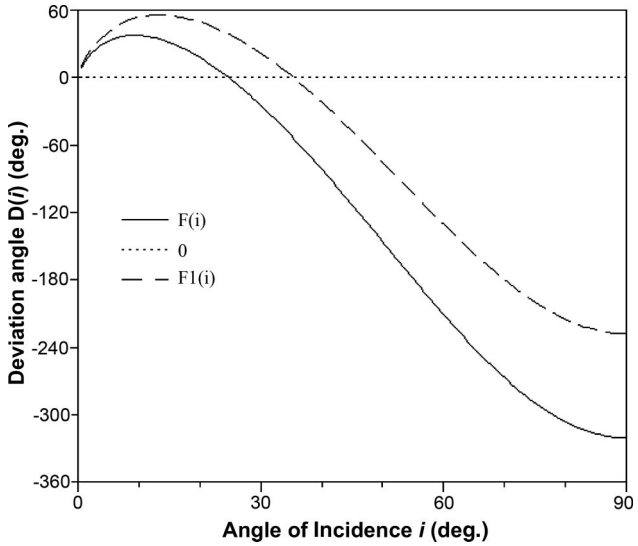

Fig. 2. $F(i)$ defined by Eq. (18a) is the incident angular component of the additional deviation incurred for the inhomogeneous sphere over that for the homogeneous one [see Eq. (18)], and is plotted for $n_0 = 5/3$. $F1(i)$ is for $n_0 = 2.5$.

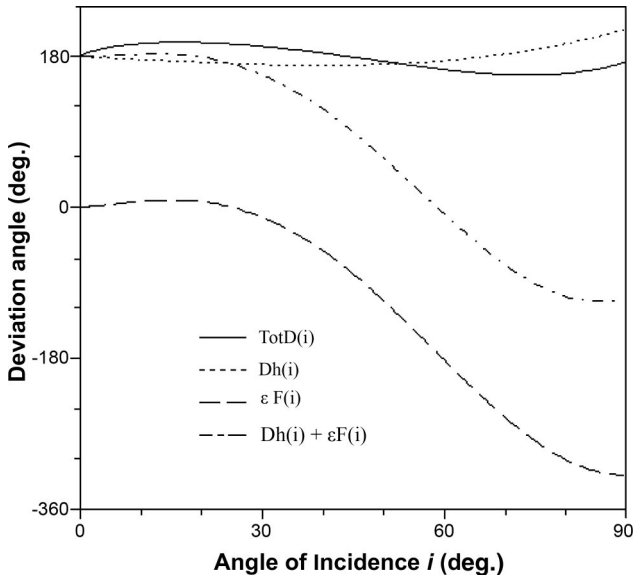

Fig. 3. Graphs of (i) the exact ray deviation TotD(i) found from Eq. (10) for the profile $\bar{n}(\lambda) = (a\lambda + b)^{-1}$ with $a = \varepsilon$ (=0.25 here) and $n_0 = 5/3$, corresponding to $n_1 = 5/(5\varepsilon + 3)$; (ii) the deviation for the homogeneous sphere Dh(i) for $\bar{n}(\lambda) = n_0 = 5/3$; (iii) the additional deviation $\varepsilon F(i)$, due to the inhomogeneity [see Eqs. (18) and (18a)]; (iv) the linear approximation to the deviation Dh(i) + $\varepsilon F(i)$, as calculated from Eq. (18).

Note that the above profile for $\bar{n}(\lambda)$ was chosen for analytic convenience; it also has the advantage that a unique value of $\bar{\lambda}$ could be specified for numerical studies. In general this is not the case. However, as noted earlier, to the extent that any profile can be approximated (sometimes quite accurately) by a linear Taylor polynomial, this result is general in that it holds for any small functional deviation from a constant profile n_0.

5. Existence of Multiple Rainbows of a Given Order

Earlier work by Brockman and Alexopoulos[27] considered ray optics for particles with refractive indices in the form of a power law; in dimensional notation $n(r) = n(R)(r/R)^m$. This functional form allows for two very unphysical situations: $n(0) = 0$ when $m > 0$ and $n(0) \to \infty$ as $\eta \to 0$ when $m < 0$. If, however, a constant index sphere of radius $a < R$ were smoothly matched to this type of profile for $a < \eta < R$, then such a composite profile might prove useful. Even without modification it represents two extreme cases of very weak and very strong central refraction respectively. For the simple power law index, Eq. (10) for $D(i)$ is reducible to a generalization of that for constant n. Unfortunately the model of Brockman *et al.* does not allow for the possibility of more than one rainbow of a given order since $D'(i)$ still possesses a unique zero i_c.

However, some insights about when this phenomenon may occur can be gained by examining the quantity $\rho(\lambda) = \lambda\bar{n}(\lambda)$ (=$\bar{K}$ = sin i) in Eq. (10). The turning point $\bar{\lambda}$ for a ray with a given angle of incidence i is given implicitly by the relation $\rho(\bar{\lambda}) = \sin i$. Figure 4

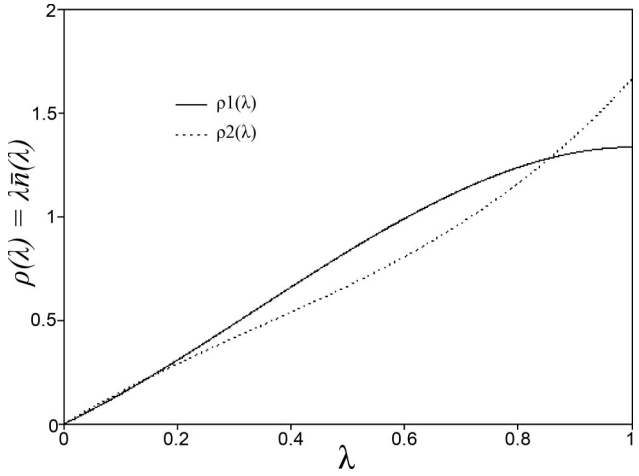

Fig. 4. Graphs of symmetric refractive index profiles.

shows two refractive index profiles: $\rho_1(\lambda) = \lambda\bar{n}_1(\lambda) = \lambda[5 - 4(\lambda - 0.5)^2]/3$ and $\rho_2(\lambda) = \lambda\bar{n}_2(\lambda) = 4\lambda[1 + (\lambda - 0.5)^2]/3$. The first corresponds to the refractive index increasing from 4/3 at $\lambda = 0$ to a maximum of 5/3 at $\lambda = 0.5$ and then decreasing back to 4/3 at the drop surface, $\lambda = 1$. The second profile corresponds to the refractive index decreasing from 5/3 at $\lambda = 0$ to a minimum of 4/3 at $\lambda = 0.5$ and then increasing back to 5/3 at the drop surface, $\lambda = 1$. The $D(i)$ graphs corresponding to these two symmetric refractive index profiles exhibit interesting differences (see Fig. 5): For $\bar{n}_1$ there is a single minimum near $i = 13.8°$ of arc, whereas for $\bar{n}_2$ there is a maximum near $i = 8.0°$ and a minimum near $i = 65.3°$—a double primary rainbow! Clearly the presence of an attractive index profile n_2 in the central region is the physical reason for this. However, despite the different concavities of both the $\bar{n}$ and the ρ profiles, there is nothing distinctive in these graphs to indicate this contrasting behavior. Perhaps this is not surprising given that it is a weighted integral of the reciprocal square root of $\rho^2 - \sin^2 i$ that is contributing to $D(i)$. It is worth noting that similar results occur for the linear profiles $n = (4 + \lambda)/3$ (minimum only) and $n = (5 - \lambda)/3$ (maximum and minimum).

Nevertheless, further insight may be gained from the more complicated profile $\bar{n}(\lambda) = [5 + \sin(6\pi\lambda)]/3$. This and the corresponding $\rho(\lambda)$ graph are shown in Fig. 6. Recall that the turning point $\bar{\lambda}$ is defined by the equation $\rho(\bar{\lambda}) = \sin i$, so the vertical axis is synonymous with $\sin i$ as far as $\bar{\lambda}$ is concerned, and therefore it is only of interest to consider $0 \le \rho \le 1$. As the angle of incidence i increases from zero to 90°, the ray will move into the sphere until it encounters the turning point $\bar{\lambda}$ and proceed no further. The axial ray ($i = 0°$) passes through the center and for $q = 1$, $\bar{\lambda}$ is obviously zero. As i increases, so too does $\bar{\lambda}$, changing slowly as a function of i at first, and more rapidly later, because the derivative of ρ, as drawn is decreasing until the point of inflection is reached. However, at the value of $\sin i$ corresponding to the

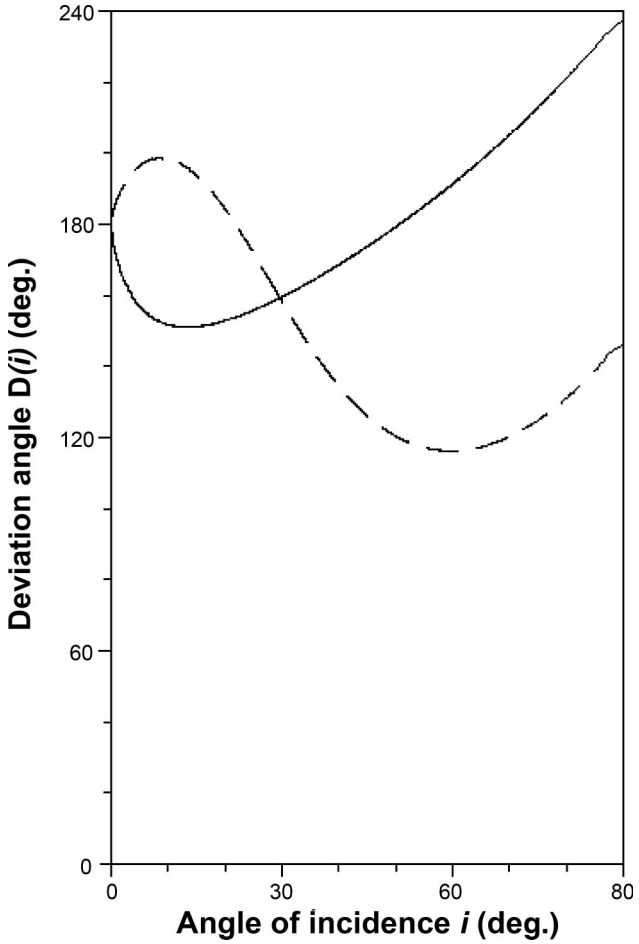

Fig. 5. Graphs of $D(i)$ for two symmetric refractive index profiles $\rho_1(\lambda)$ and $\rho_2(\lambda)$.

relative minimum of $\rho(\bar{\lambda})$, $\bar{\lambda}$ jumps discontinuously on this graph from approximately 0.39 to about 0.57 and then climbs to approximately 0.64 when $i = 90°$. If instead of starting at i equal to zero we had reversed the process, starting with a tangentially incident ray ($\sin i = 1$), the track of $\bar{\lambda}$ is reversible. At the relative minimum of $\rho(\bar{\lambda})$, this being the coalescence of two turning points (the inner one being inaccessible to an incoming ray), we might expect some correspondingly aberrant behavior in $D(i)$, and this does indeed occur (see Fig. 7). The spiked behavior evident in this figure is therefore associated with the discontinuity in the turning point $\bar{\lambda}(i)$.

Another feature is noteworthy. It appears that for at least monotonically decreasing $n(r)$ profiles, the quantity

$$L(i) = \bar{K}\int_{\bar{\lambda}}^{1} \frac{d\lambda}{\lambda\sqrt{\lambda^2\bar{n}^2(\lambda) - \bar{K}^2}} \tag{20}$$

possesses a point of inflection, while for monotonically increasing profiles it does not, exhibiting only a graph with upward concavity. Furthermore it is apparent from Fig. 8 (drawn for a linearly decreasing refractive index profile) that the derivative $L'(i)$ is

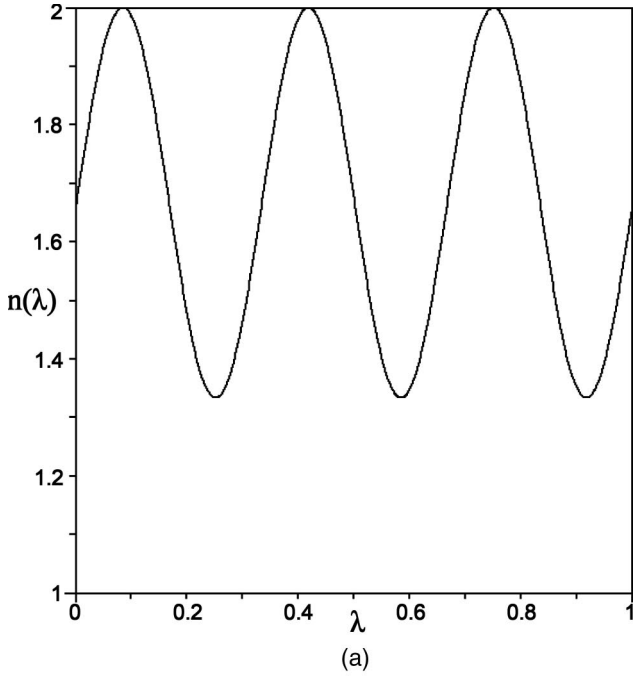

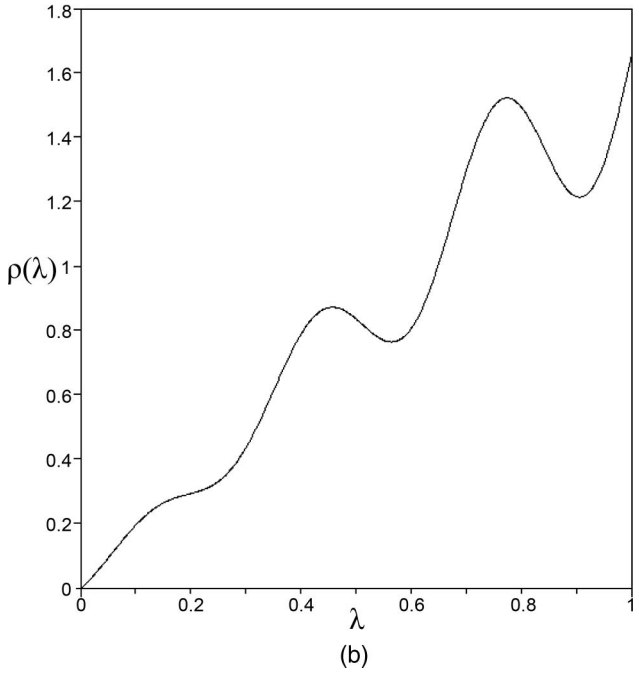

Fig. 6. (a) Variation of refractive index $n(\lambda)$ as a function of the normalized radius λ of the sphere. (b) Variation of singular point $\rho(\lambda)$ as a function of the normalized radius λ of the sphere.

negative in the interval of interest. These are obviously necessary conditions for the existence of double extrema in the graph of $D(i)$, since the remaining terms are linear in i. This feature is also present for the parabolic profile $n(r) = 4[1 + (r - 0.5)^2]/3$, so it appears that the double bow exists provided the profile is sufficiently attractive in the deep interior of the drop.

Nevertheless, these general criteria on $L(i)$ are still insufficient to translate into conditions on $n(r)$. In the graphs below for $n(\lambda) = (5 - \lambda)/3$ (Fig. 8), $D(i)$ is the total deviation [Eq. (10)] and $Dl(i)$ is just the linear part of $D(i)$, namely $Dl(i) = 2i$.

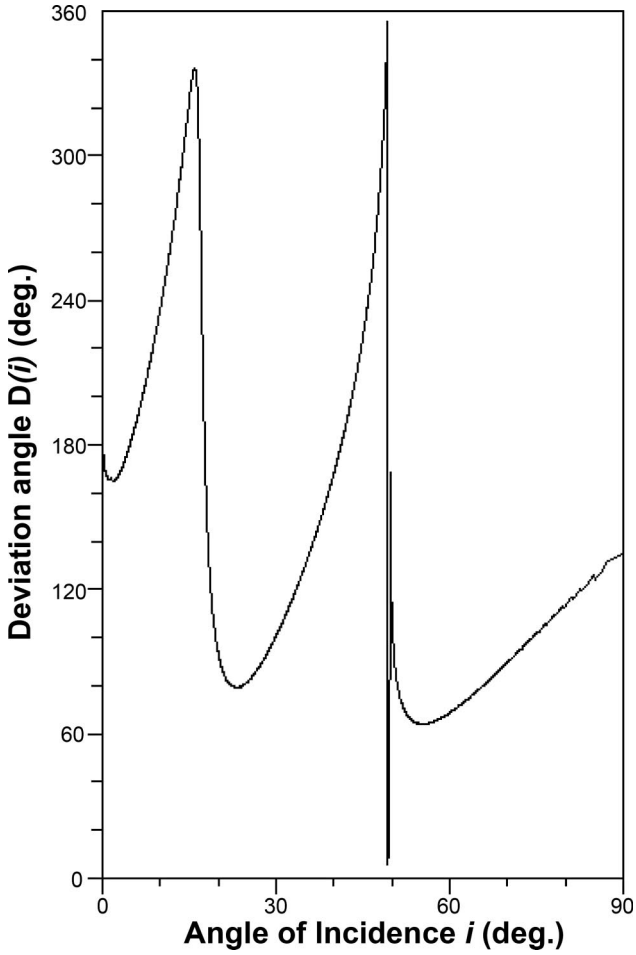

Fig. 7. Graph of $D(i)$ for $\bar{n}(\lambda) = [5 + \sin(6\pi\lambda)]/3$. Note the multiple extrema and also the apparent singular behavior near $i \approx \arcsin 0.76 = 49.5°$, corresponding to the smallest minimum of $\rho(\lambda)$ in Fig. 6.

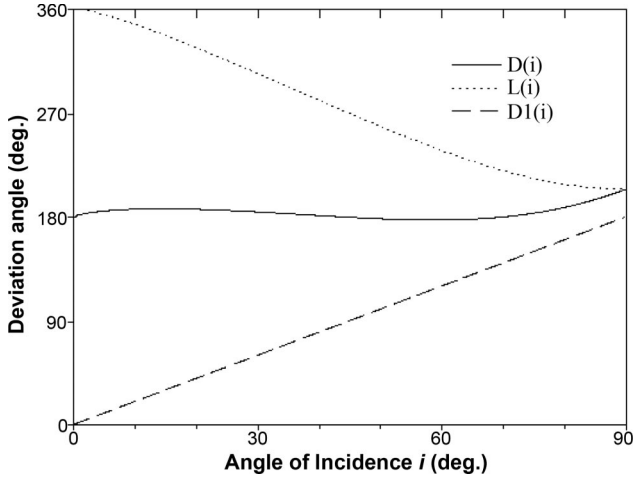

Fig. 8. Graphs of (i) $D(i)$ as given by Eq. (10), (ii) the integral term $L(i)$ as defined by Eq. (24), and (iii) the linear part of $D(i)$, namely $Dl(i) = 2i$, where $D(i) = Dl(i) + 4L(i) - \pi$.

6. Conclusion

A ray-theoretic account of the passage of light through a radially inhomogeneous transparent sphere has been used to establish the existence of multiple (≥ 2) primary rainbows (and in principle, higher-order bows) for some refractive index profiles. The existence of such additional bows is a consequence of a sufficiently attractive potential in the interior of the drop, i.e., the refractive index gradient should be sufficiently negative there. Further work is required to quantify the adjective "sufficiently" in the previous sentence. The profiles for which this gradient is monotonically increasing do not result in this phenomenon, but nonmonotone profiles can do so, depending on the form of n. Indeed, sufficiently oscillatory profiles can lead to apparently singular behavior in the deviation angle (within the geometrical optics approximation) as well as to multiple rainbows.

References

1. C. L. Adler, J. A. Lock, I. P. Rafferty, and W. Hickok, "Twin-rainbow metrology. I. Measurement of the thickness of a thin liquid film draining under gravity," Appl. Opt. **42,** 6584–6594 (2003).
2. C. W. Chan and W. K. Lee, "Measurement of a liquid refractive index by using high-order rainbows," J. Opt. Soc. Am. B **13,** 532–535 (1996).
3. H. Hattori, H. Yamanaka, H. Kurniawan, S. Yokoi, and K. Kagawa, "Using minimum deviation of a secondary rainbow and its application to water analysis in a high-precision refractive-index comparator for liquids," Appl. Opt. **36,** 5552–5556 (1997).
4. H. Hattori, K. Kakui, H. Kurniawan, and K. Kagawa, "Liquid refractometry by the rainbow method," Appl. Opt. **37,** 4123–4129 (1998).
5. H. Hattori, "Simulation study on refractometry by the rainbow method," Appl. Opt. **38,** 4037–4046 (1999).
6. J. Hom and N. Chigier, "Rainbow refractometry: simultaneous measurement of temperature, refractive index, and size of droplets," Appl. Opt. **41,** 1899–1907 (2002).
7. C. L. Adler, J. A. Lock, and B. R. Stone, "Rainbow scattering by a cylinder with a nearly elliptical cross section," Appl. Opt. **37,** 1540–1550 (1998).
8. C. L. Adler, J. A. Lock, D. Phipps, K. Saunders, and J. Nash, "Supernumerary spacings of rainbows produced by an elliptical cross-section cylinder. II: Experiment," Appl. Opt. **40,** 2535–2545 (2001).
9. P. Massoli, "Rainbow refractometry applied to radially inhomogeneous spheres: the critical case of evaporating droplets," Appl. Opt. **37,** 3227–3235 (1998).
10. M. Schneider and E. D. Hirleman, "Influence of internal refractive index gradients on size measurements of spherically symmetric particles by phase Doppler anemometry," Appl. Opt. **33,** 2379–2388 (1994).
11. M. Schneider, E. D. Hirleman, H. Salaheen, D. Q. Choudury, and S. C. Hill, "Rainbows and radially inhomogeneous droplets," in *Proceedings of the Third International Congress on Optical Particle Sizing,* M. Maeda, ed. (Yokohama, 1993), pp. 323–326.
12. P. Massoli, "Temperature and size of droplets inferred by light scattering methods: a theoretical analysis of the influence of internal inhomogeneities," presented at the *13th Annual Conference on Liquid Atomization and Spray Systems* (ILASS-Europe, Florence, 1997).
13. L. Kai, P. Massoli, and A. D'Alessio, "Some far-field scattering characteristics of radially inhomogeneous particles," Part. Part. Syst. Charact. **11,** 385–390 (1994).
14. P. L. Marston, "Rainbow phenomena and the detection of nonsphericity in drops," Appl. Opt. **19,** 680–685 (1980).
15. J. P. A. J. van Beeck and M. L. Riethmuller, "Rainbow phenomena applied to the measurement of droplet size and velocity and to the detection of nonsphericity," Appl. Opt. **35,** 2259–2266 (1996).
16. J. P. A. J. van Beeck and M. L. Riethmuller, "Nonintrusive measurements of temperature and size of single falling raindrops," Appl. Opt. **34,** 1633–1639 (1995).
17. K. Anders, N. Roth, and A. Frohn, "Influence of refractive index gradients within droplets on rainbow position and implications for rainbow refractometry," Part. Part. Syst. Charact. **13,** 125–129 (1996).
18. N. Roth, K. Anders, and A. Frohn, "Size insensitive rainbow refractometry: theoretical aspects," presented at the *Eighth International Symposium on Applications of Laser Techniques to Fluid Mechanics* (Lisbon, 1996).
19. J. W. Y. Lit, "Radius of uncladded optical fiber from back-scattered radiation pattern," J. Opt. Soc. Am. **65,** 1311–1315 (1975).
20. D. Marcuse, "Light scattered from unclad fibers: ray theory," Appl. Opt. **14,** 1528–1532 (1975).
21. H. M. Presby, "Refractive index and diameter measurements of unclad optical fibers," J. Opt. Soc. Am. **64,** 280–284 (1974).
22. M. R. Vetrano, J. P. A. J. van Beeck, and M. L. Riethmuller, "Generalization of the rainbow Airy theory to nonuniform spheres," Opt. Lett. **30,** 658–660 (2005).
23. M. R. Vetrano, J. P. A. J. van Beeck, and M. L. Riethmuller, "Assessment of refractive index gradients by standard rainbow thermometry," Appl. Opt. **44,** 7275–7281 (2005).
24. M. Born and E. Wolf, *Principles of Optics* (Cambridge U. Press, 2002).
25. R. K. Luneberg, *Mathematical Theory of Optics* (U. California Press, 1966).
26. I. S. Gradshteyn and I. M. Ryzhik, *Table of Integrals, Series and Products* (Academic, 1980).
27. C. L. Brockman and N. G. Alexopoulos, "Geometrical optics of inhomogeneous particles: glory ray and the rainbow revisited," Appl. Opt. **16,** 166–174 (1977).